Electronic Supporting Information

Electrochemically grown nanoporous MnO_2 nanowall forest on porous carbon substrate with enhanced capacitance through faster ionic and electrical mobility

Bihag Anothumakkool, Sreekumar Kurungot

Physical & Materials Chemistry Division, CSIR-National Chemical Laboratory,
Pune-411008, Maharashtra, India.
Phone: 91-20-25902566, Fax: 91-20-25902636
E-mail: k.sreekumar@ncl.res.in

Experimental section:

Materials: Manganese acetate ($MnAc_2$), ammonium acetate (NH_4Ac) and sodium sulfate (Na_2SO_4) were purchased from Rankem Chemicals. All the chemicals were used as received without any further purification. Carbon paper having a thickness of 0.3 mm was purchased from Toray.

Preparation MnO_2 coated carbon paper: Electrochemical synthesis was carried out in Bio-Logic SP-300 Potentio-Galvanostat using 3-electrode systems in which carbon paper was used as the working electrode, Pt was used as the counter electrode and Ag/AgCl was used as the reference electrode. Deposition was carried out in a solution containing 0.1 M (0.49 g) $Mn(Ac)_2$ and 0.1 M (0.154 g) NH_4Ac salt in 20 ml of deionized water. 1 cm^2 area of carbon paper was kept exposed to electrolyte and the remaining part was masked using Kapton adhesive tape. Experiments were carried out at a constant potential of 0.6 V Vs Ag/AgCl for different time intervals. Carbon paper was dipped in ethanol before electro-deposition to enhance the hydrophilic nature. After the deposition, the electrode was washed and dried at 60 ^{o}C.

The amount of MnO_2 deposited was calculated by using Faraday's law of electrolysis:

$$W = \frac{\text{Charge passed (C)} * 87\text{(Mol. weight of MnO2)}}{96\,485 * 2 \text{ (no electron released per MnO2)}}$$

For comparison purpose, MnO_2/CNF was also prepared. In a typical experiment, 100 mg of CNF and 150 mg of $KMnO_4$ were dispersed in 40 mL water using a probe sonicator. The solution was poured into a hydrothermal bomb and was kept at 140 ^{o}C for 24 h followed by filtration. Filtrate was washed and kept for drying at 60 ^{o}C.

Characterisation

Structure and morphology of the materials were analyzed using Nova Nano SEM 450 and Quanta™ Scanning Electron Microscope. High-resolution transmission electron microscope (HR-TEM) was carried out in Tecnai-T 30 at an accelerated voltage of 300 kV. The X-ray diffraction patterns of the prepared specimens were done using PAN X'pert Pro instrument, data collection was done at a scan rate of 1.5 ^{o}/min using Cu Kα radiation. Raman analysis was carried out on Horiba Jobin Yvon Inverted LabRAM HR800 VIS-NIR using 632 nm solid-state diode laser beams. X-ray Photoelectron Spectroscopic (XPS) measurements were carried out on a VG Micro Tech ESCA 300° instrument at a pressure of $> 1 \times 10^{-9}$ Torr (pass energy of 50 eV, electron take off angle of 60^{o} and the overall resolution of ~ 0.1 eV). Nitrogen adsorption-desorption experiments were conducted at 77 K using Quantachrome Quadraorb automatic volumetric instrument. Before gas adsorption measurements, the sample was activated at room temperature (for 24 h) and 100 ºC (for 36 h) under ultrahigh vacuum (10-8 mbar) for overnight. The deposited MnO_2 was carefully scratched from the carbon surface and analyzed for gas adsorption, except in the experiments as shown in SI, Figure S9 and Figure S2b, where the gas adsorption was done on the carbon paper. Surface area is calculated from the N_2-adsorption isotherm up to 0.3 relative pressures. Pore size distribution is calculated by the DFT method.

Electrochemical Characterization: All the electrochemical studies were carried out in a BioLogic SP-300 Potentio-Galvanostat. Metal crocodile clips were used for the required electrical contacts from the electrodes. Cyclic Voltammetry (CV) was carried out in a 3-electrode setup where MnO_2 coated carbon paper was used as a working electrode and Ag/AgCl was used as a reference electrode and Pt mesh as counter electrode. The CV measurements were taken at different scan rates from 10 to 1500 mV/s by maintaining a potential window between 0 to 1 V *Vs* Ag/Agcl. Mass specific capacitance of MnO_2 is calculated from the CV using the following equation[1]

$$Q(charge) = \frac{\int_{E1}^{E2} I(E)dE}{v} \text{ -------------------- (1)}$$

Where

$E_1 - E_2$= Potential window

m = Weight of the MnO_2 coated in one of the electrodes (g)

v = Scan rate (mV/s)

Capacitance is calculated from the chrono charge discharge method using the following equation

$$\mathrm{C} = \left(\frac{I\Delta t}{\Delta V * M}\right) \text{------------------------- (3)}$$

Where

Δt = Discharge time
ΔV = Potential window
I = Constant current used for charging and discharging
M = Weight of active electrode material in the electrode.

The charge-discharge measurement was done at different current densities (1 to 100 A/g) in the same potential range which was used for CV. Cycling stability was done by chrono charge-discharge method at 5 A/g current density for 1000 continuous cycles. Coulombic efficiency is calculated during the charge-discharge cycling by taking the percentage of charging time coulombs by discharge coulombs. Electrochemical impedance (EIS) analysis was carried out from 10^6 Hz to 0.01 Hz frequency against the open circuit potential with a sinus amplitude of 10 mV (Vrms = 7.07 mV). All the EIS data were analyzed using an EC-Lab Software V10.19.

Asymmetric capacitor was assembled by using activated carbon (AC) as the negative electrode and MnO_2/carbon paper as the positive electrode. AC was made into a paste with conducting carbon and binder in a ratio of 80:15:5 in N-methyl 2-pyrrolidone. The above made paste was brush coated to the carbon paper with an area of 1 cm^2 and the loading was adjusted according to the specific capacitance of AC (180 F/g). Measurements were carried out in 1M Na_2SO_4

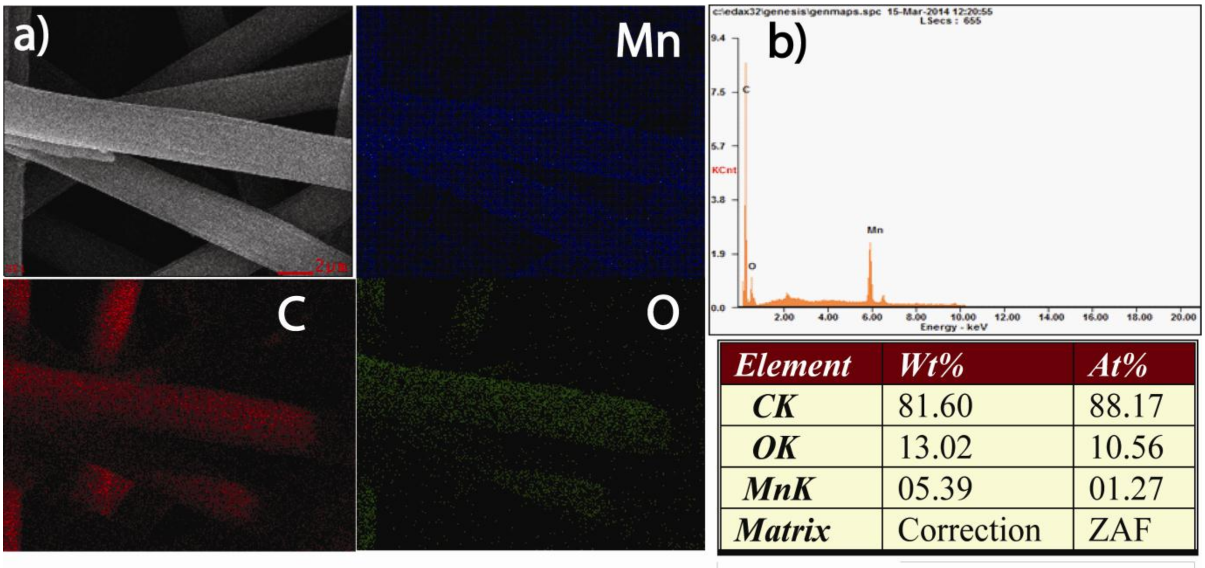

Element	***Wt%***	***At%***
CK	81.60	88.17
OK	13.02	10.56
MnK	05.39	01.27
Matrix	Correction	ZAF

Figure S1: a) EDAX elemental mapping of the MnO_2 nanowalls, b) EDAX spectra and the table indicating the % of elements present in the area of Figure S1a.

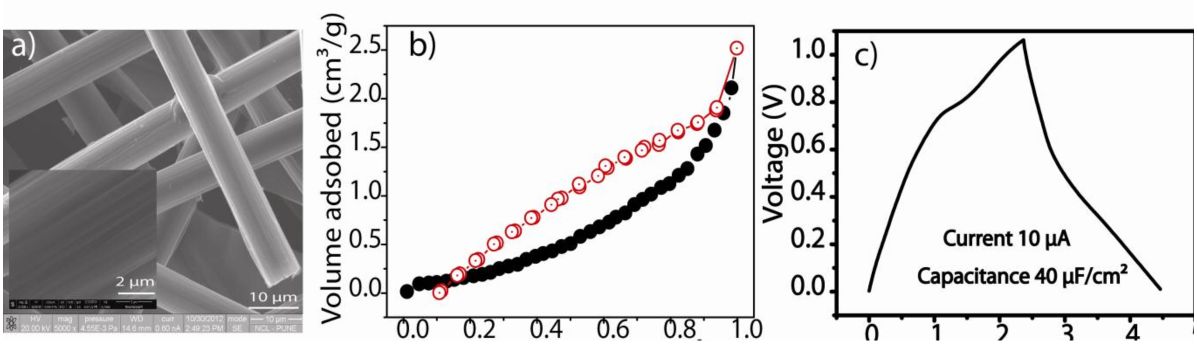

Figure S2: a) SEM images of the carbon fiber paper with zoomed images of a single fiber in the inset, b) nitrogen adsorption isotherm of the carbon fiber paper and c) charge-discharge profile of bare carbon fiber paper.

SEM image of the carbon fiber paper clearly indicate the smooth fibers with 5-7 µm diameter **(Figure S2a)**. Inset of Figure S2a show a single fiber indicating the smooth surface. BET surface area measurement shows merely 1 m^2/g surface area for the paper which indicates there is now pores at nano regime (**Figure S2b**). **Figure S2c** also includes the charge-discharge profile of bare carbon paper which shows a capacitance of 40 $\mu F/cm^2$ and thus negligible contribution from the support towards the total capacitance. Thus, highly porous carbon paper compared to a plane current collector helps for the high mass loading of MnO_2 but at the same time it gives adequate conducting support.

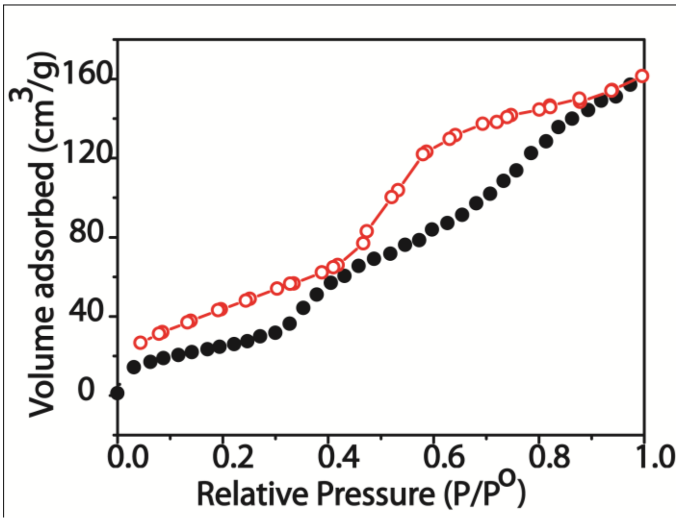

Figure S3: Nitrogen adsorption isotherm of Mn/CP-300.

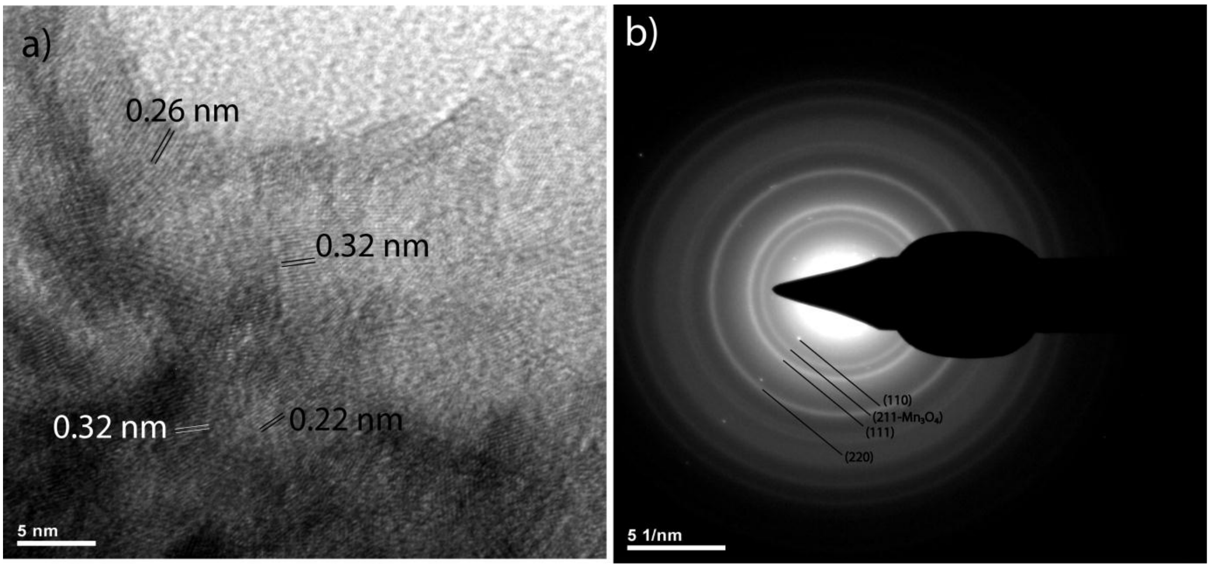

Figure S4. a) High-resolution TEM (HR-TEM) image of MnO_2 (different crystal planes are marked by lines); b) SAED image of MnO_2 nanowalls.

HRTEM (Figure S4a) images clearly show partial crystallinity in the selected area. This was contradictory to the XRD spectra (Figure S5c), which lack characteristic peaks of MnO_2 probably due to the high amorphous content. Selected area diffraction (SAED) pattern in Figure S4b shows (110), (111) and (220) planes corresponding to the d-spacing of 0.32, 0.26 and 0.15 nm which are also found to in accordance with the values deduced from the

HRTEM image presented in Figure S4a[2]. A d-spacing of 0.22 nm indicates the presence of the crystal plane (211), which can probably be due to the presence of Mn_3O_4. Presence of this phase is also confirmed from the Raman spectra. Thus, XRD, HRTEM and SAED results show high amount of amorphous MnO_2 in the nanowalls with partial crystalline phase which is difficult to ascertain to a particular MnO_2 phase due to polycrystalline nature as indicated by the SAED images.

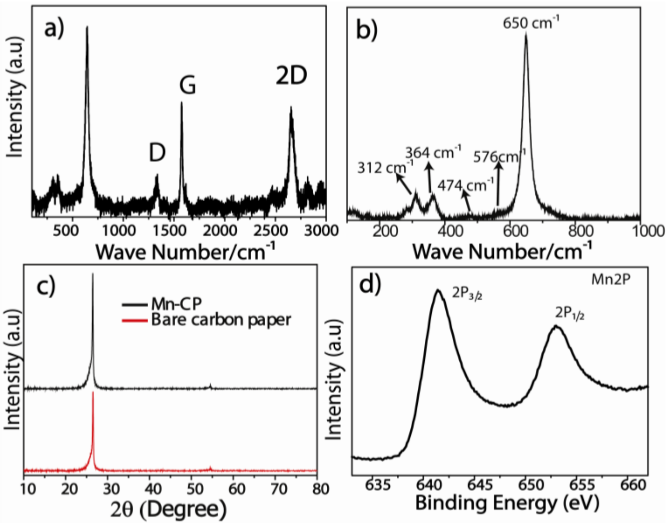

Figure S5: a) Full scale Raman spectrum, b) enlarged view of the spectrum below 1000 cm^{-1} where the characteristic MnO_2 peaks are present, c) XRD spectra and d) Mn2p XPS; the measurements are done by using the MnO_2 coated carbon paper.

Raman spectrum scanned between 100-1000 cm^{-1} (**Figure S5a and b**) shows a strong peak at 650 cm^{-1} due to the symmetric stretching vibration of Mn-O[3]. Two weak peaks are also observed at 576 and 474 cm^{-1} in which the former one is due to the stretching of the basal plane of MnO_2[3a]. Above peaks indicate the presence of birnessite-type of MnO_2 in the nanowalls. Raman spectrum also indicates the presence of Mn_3O_4 phase due to the peaks obtained at 312 and 364 cm^{-1} which correspond to the T2g, and Eg active modes of Mn_3O_4 apart from the normal MnO_2 peaks[4].

Mn 2P X-ray photoelectron spectrum (XPS) is shown in **Figure S5d.** It possesses two peaks at 653.0 and 642.4 eV respectively which are corresponding to $2P_{3/2}$ and $2P_{1/2}$ with a binding energy difference of 11.58 eV. These values are very similar to the reported values in the literature[5].

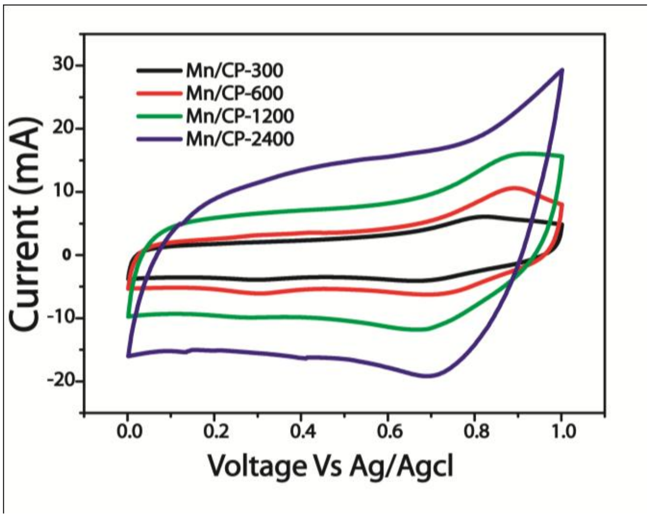

Figure S6: Combined cyclic voltammograms of Mn/CP-300 to Mn/CP-2400 carried out at a scan rate of 50 mV/s in 1M Na_2SO_4.

Table.1: Comparison of the charge storage properties of the present porous MnO_2 nanowall system with the recent literature reports involving electrodeposited MnO_2 electrodes.

Material	Loading mg/cm^2	C_s F/g	Current Density/scan rate	Potential Window (V)	Electrolyte	Reference
Porous MnO_2 nanowalls	0.135	1149	1 A/g	0.8	1M $NaSO_4$	This work
		769	10 A/g			
		797	5 mV/s			
		505	200 mV/s			
	0.27	790	2 A/g			
		534	10 A/g			
		589	5mV/s			
		324	200 mV/s			
MnO_2	0.23	1058 95	0.74 A/g 10 A/g	0.8	1M $NaSO_4$	2a
"	0.06	420 180	5 mV/s 200 mV/s	0.9	0.5 M Na_2SO_4	5b
MnO_2/PEDOT /Graphene		380 180	0.1 mA/cm^2 5 mA/cm^2	0.85	"	6
MnO_2/CNT/sponge	0.1	444 295	1 mV/s 100 mV/s	1	1M Na_2SO_4	7
Graphene/MnO_2 textile	0.27	315 120	2 mV/s 100 mV/s	0.85	0.5 M Na_2SO_4	8
WO3–x@Au@MnO_2	0.27	588 220	10 mV/s 100 mV/s	0.8	0.1M Na_2SO_4	*9*
Au/MnO_2	0.025	750 525	5 mV/s 100 mV/s	0.9	2M Li_2SO_4	10
MnO_2 Nano pillar	0.14	603 320	5 mV/s 100 mV/s	0.8	1M Na_2SO_4	*11*
MnO_2	0.27	425	5 A/g	1.2	1M $LiClO_4$	*12*

nanofiber/carbon cloth		300	40 A/g			
MnO_2/Ti nitride nanotube coaxial arrays	0.06	681	2 A/g	0.8		[5a]

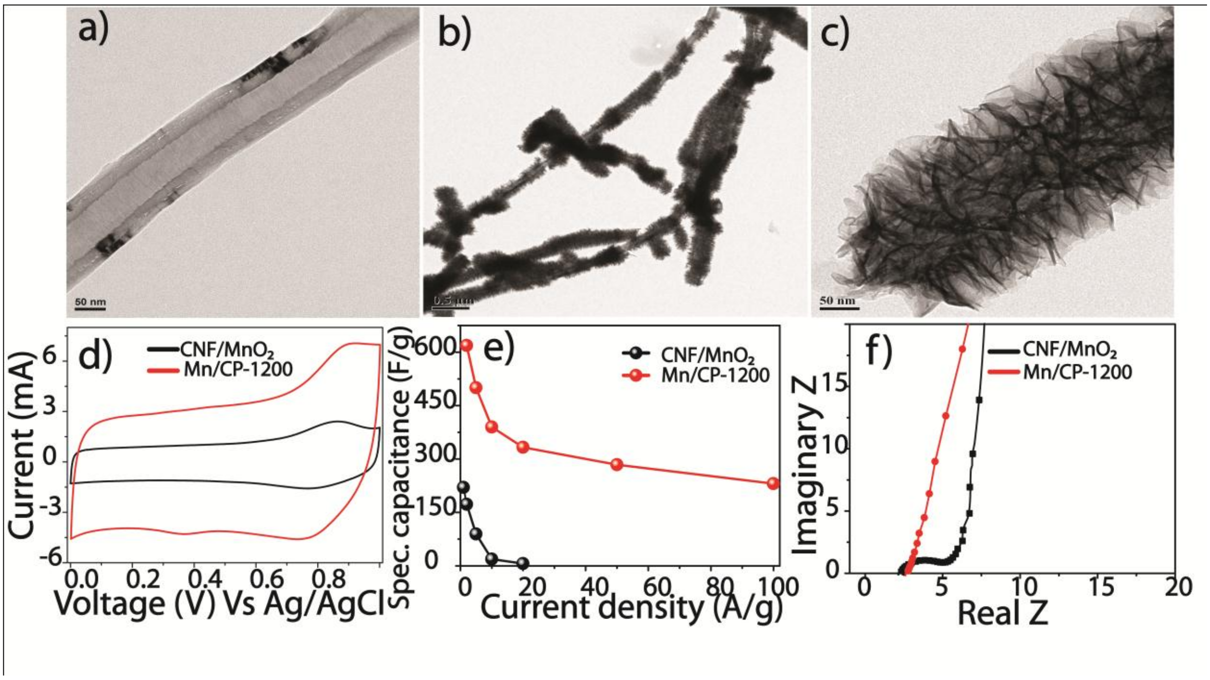

Figure S7: TEM image of a) bare CNF, b) & c) CNF/MNO_2 composites, d) cyclic voltammograms of CNF/MnO_2 and Mn/CP-1200 recorded at 50 mV/s e) specific capacitance measured at varies current densities and f) comparative Nyquist plot of CNF/MnO_2 and Mn-CP-1200.

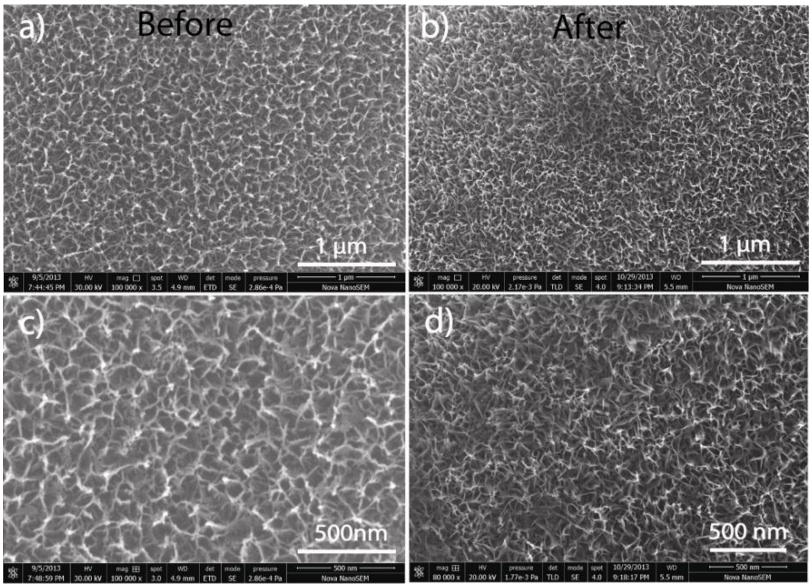

Figure S8: FE-SEM images of a) & c) before and b) & d) after the stability cycles.

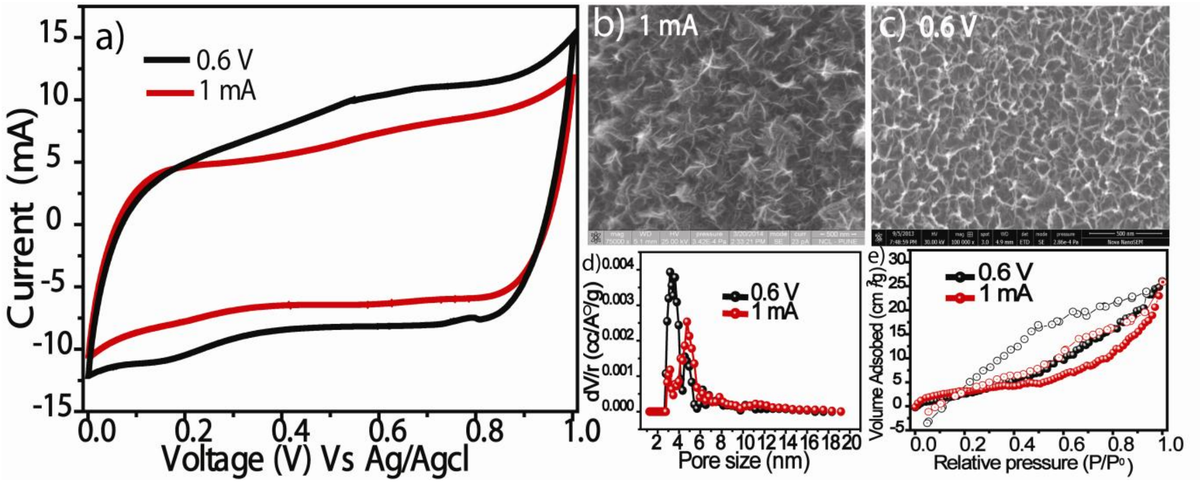

Figure S9. a) Cyclic voltammograms recorded at 50 mV/s for MnO_2 nanowalls forest which was deposited at 0.6 V (black line) and nanoflower formed at 1 mA deposition (red line), b) & c) corresponding SEM images for the MnO_2 nanoflower and nonowall forest formed at different deposition conditions, d) pore distribution patterns for the MnO_2 naowflower and nanowall forest obtained at different deposition conditions and e) N_2-adsorptoion isotherms recorded over the MnO_2 nanoflower and nanowall forest.

Structure and morphology of MnO_2 formed clearly depend on various factors. During electrodeposition, apart from the selected precursors, the derived structure also has dependency on the mode of deposition (constant current or potential), amount of current passed per second and the nature of the substrate as well. To testify this, we had controlled the electro-deposition process by maintaining two conditions in which the amount of charge passed remains the same (1200 mC). This includes (**Case-I**) deposition at constant potential (i.e. chrono-amperometry, 0.6 V Vs Ag/AgCl) and (**Case-II**) deposition at constant current (i.e. chrono-potentiometry 1 mA). SEM images of the formed MnO_2 in both the cases are shown in the **Figure S9** which clearly indicates that the morphology quite varies with the method adopted for electro-deposition. Compared to the nanowall forest in **Case-I**, which was obtained at 0.6 V, **Case-II** shows nanoflower structure. Surface area obtained for the material formed in **Case-I** is 19 m^2/g and in **Case-II** is 12 m^2/g (**Figure S9e;** this includes the weight of carbon paper and MnO_2. The carbon paper alone shows a surface area of 1 m^2/g (**Figure S2b**). Apart from this, the pore volume is 1.5 times lower in the case of the nanoflower formed in **Case-II** compared to the nanowall forest formed in **Case-I** (**Figure S9d**). This unambiguously confirms that the nanowall architecture possesses high surface area with perfect pore distribution, which helps for attaining high specific capacitance (**Figure S9a**). At 0.6 V, the reaction is limited by the diffusion of Mn^{2+} due to the high oxidation potential which results in high current of 15 mA in the beginning and decrease gradually to 2-5 mA. Thus, since the potential is controlled throughout the experiment in **Case-I**, the diffused Mn^{2+} ions will be consumed fast and be grown vertically were nucleation starts rather filling in the vacant space. We believe that this diffusion controlled electrodeposition is the reason for the formation of nanowalls [13]. On the other hand, in **Case-II**, due to the low current of 1 mA, there is no such diffusion limitation. At 0.6 V (**Case-I**), we also observed oxygen evolution at small rates, which is also expected to have a role in controlling the growth pattern and porosity of the system.

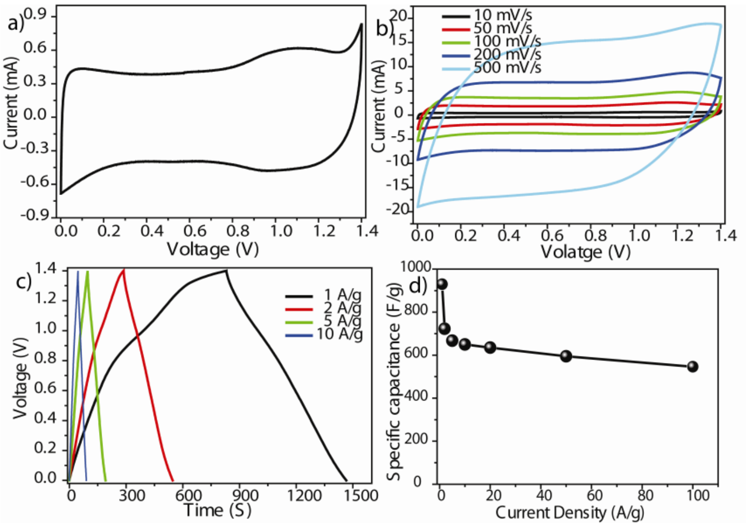

Figure S10: Charge storage properties of an asymmetric capacitor using Mn/CP-300: a) cyclic voltammogram recorded at a scan rate of 10 mV/s, b) the CV profiles obtained at various scan rates, c) charge discharge profiles and d) specific capacitance at varied scan rates.

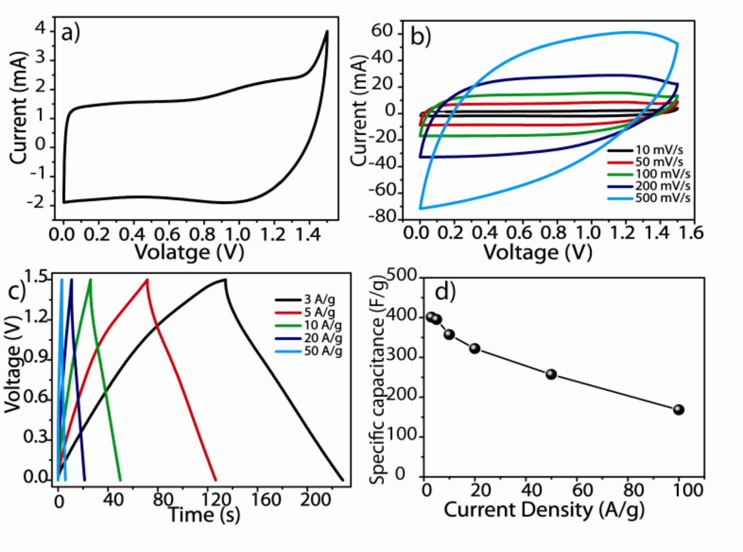

Figure S11: Charge storage properties of an asymmetric capacitor using Mn/CP-2400: a) cyclic voltammogram recorded at a scan rate of 10 mV/s, b) the CV profiles taken at various scan rates, c) charge discharge profiles and d) specific capacitance at varied scan rates.

Even though we had shown a high specific capacitance of 1149 F/g for Mn/CP-300 in a 3-electrode fashion, its reproducibility in an actual supercapacitor which works in 2-electrode fashion is very important. Here, we have carried out two sets of experiments by using Mn/CP-300 (where the mass loading is 0.135 mg/cm^2) and Mn/CP-1200 (where the mass loading is 1 mg/cm^2) as the positive electrodes. To utilise the full ability of the asymmetric capacitor, we increased the potential window from 1 V to 1.4 V. It is interesting to note that still Mn/CP-300 in the 2-electrode configuration shows a high specific capacitance of 930 F/g. Also, even at 100 A/g current density, 60% of its initial capacitance is retained. Details are given **SI Figure 10**. In the case of Mn/CP-2400, where we could achieve a mass loading of 1 mg/cm^2, a capacitance of 402 F/g in a potential window 1.5 V could be achieved. The above obtained capacitance of Mn/CP-2400 is even slightly higher than the obtained capacitance (340 F/g) in a 3-electrode system. Thus, the obtained capacitance of nanowall forest indicates its prospects for devise applications. Details of charge storage measurement are shown in **Figure S11**. In case of Mn/CP-300 oxygen evolution restrict the window around 1.4 V due to oxygen evolution.

References

1. W. Chen, Z. Fan, L. Gu, X. Bao and C. Wang, *Chem. Commun.*, 2010, 46, 3905-3907.
2. (a)L. Mai, H. Li, Y. Zhao, L. Xu, X. Xu, Y. Luo, Z. Zhang, W. Ke, C. Niu and Q. Zhang, *Sci Rep*, 2013, 3, 1718; (b)S. Devaraj and N. Munichandraiah, *J. Phys. Chem. C*, 2008, 112, 4406-4417.
3. (a)Y.-K. Hsu, Y.-C. Chen, Y.-G. Lin, L.-C. Chen and K.-H. Chen, *Chem. Commun.*, 2011, 47, 1252-1254; (b)J. Luo, H. T. Zhu, H. M. Fan, J. K. Liang, H. L. Shi, G. H. Rao, J. B. Li, Z. M. Du and Z. X. Shen, *J. Phys. Chem. C*, 2008, 112, 12594-12598.
4. Z.-Y. Tian, P. Mountapmbeme Kouotou, N. Bahlawane and P. H. Tchoua Ngamou, *J. Phys. Chem. C*, 2013, 117, 6218-6224.
5. (a)S. Dong, X. Chen, L. Gu, X. Zhou, L. Li, Z. Liu, P. Han, H. Xu, J. Yao, H. Wang, X. Zhang, C. Shang, G. Cui and L. Chen, *Energy & Environmental Science*, 2011, 4, 3502-3508; (b)L. Hu, W. Chen, X. Xie, N. Liu, Y. Yang, H. Wu, Y. Yao, M. Pasta, H. N. Alshareef and Y. Cui, *ACS Nano*, 2011, 5, 8904-8913.
6. G. Yu, L. Hu, N. Liu, H. Wang, M. Vosgueritchian, Y. Yang, Y. Cui and Z. Bao, *Nano Lett*, 2011, 11, 4438-4442.
7. W. Chen, R. B. Rakhi, L. Hu, X. Xie, Y. Cui and H. N. Alshareef, *Nano Lett*, 2011, 11, 5165-5172.
8. G. Yu, L. Hu, M. Vosgueritchian, H. Wang, X. Xie, J. R. McDonough, X. Cui, Y. Cui and Z. Bao, *Nano Lett*, 2011, 11, 2905-2911.
9. X. Lu, T. Zhai, X. Zhang, Y. Shen, L. Yuan, B. Hu, L. Gong, J. Chen, Y. Gao, J. Zhou, Y. Tong and Z. L. Wang, *Adv. Mater.*, 2012, 24, 938-944.
10. J. Kang, A. Hirata, L. Kang, X. Zhang, Y. Hou, L. Chen, C. Li, T. Fujita, K. Akagi and M. Chen, *Angew Chem Int Ed Engl*, 2013, 52, 1664-1667.
11. Z. Yu, B. Duong, D. Abbitt and J. Thomas, *Adv Mater*, 2013, 25, 3302-3306.
12. M.-S. Wu, Z.-S. Guo and J.-J. Jow, *J. Phys. Chem. C*, 2010, 114, 21861-21867.
13. S. I. Cho and S. B. Lee, *Acc. Chem. Res.*, 2008, 41, 699-707.